

Observation of in-plane anisotropy of vortex pinning by inclined columnar defects

Th. Schuster, M. V. Indenbom,* H. Kuhn, and H. Kronmüller

Max-Planck-Institut für Metallforschung, Institut für Physik, Postfach 800665, D-70506 Stuttgart, Germany

M. Leghissa and G. Kreiselmeyer

Physikalisches Institut, Universität Erlangen-Nürnberg, Erwin-Rommel-Straße 1, D-91058 Erlangen, Germany

(Received 9 May 1994)

The anisotropy of the critical current density introduced in the (a, b) plane of $\text{DyBa}_2\text{Cu}_3\text{O}_{7-\delta}$ single crystals by oblique irradiation with heavy ions is observed by magneto-optics. The pinning forces on vortices oriented perpendicular to the (a, b) plane are largest when directed perpendicular to the columnar defects. Two modes of vortex motion are considered. Effects of flux creep and thermal depinning on the critical current density are discussed.

Pinning of flux lines by various types of material defects is one of the most interesting features both for the application and theoretical understanding of superconductors. In high-temperature superconductors (HTSC's), large critical current densities and large pinning energies may be achieved when columnar defects are introduced by heavy ion irradiation.¹⁻⁶ According to theoretical estimates⁷ if the full length of each vortex is pinned by the columnar defects the critical current density j_c can almost reach the depairing current density

$$j_d = \frac{\Phi_0}{3\sqrt{3}\pi\mu_0\lambda^2(T)\xi(T)} \approx \frac{R}{\xi(T)} j_c, \quad (1)$$

where Φ_0 is the flux quantum, λ the penetration depth, ξ the coherence length, and R the radius of the columnar defects. However, it was recently found³ in $\text{Bi}_2\text{Sr}_2\text{CaCu}_2\text{O}_{8+\delta}$ (BSCCO) that the experimentally determined critical current density is smaller than $(\xi/R)j_d$ [Eq. (1)] and the experimentally measured activation energy U is smaller than the theoretical value if the full length of the flux line is depinned. This discrepancy between the theoretical and experimental values of activation energies of BSCCO was explained by assuming that the vortex lines dissolve into pancake vortices.³ Even in the less anisotropic $R\text{Ba}_2\text{Cu}_3\text{O}_{7-\delta}$ (R = rare earth metal) superconductors the measured j_c is smaller than $(\xi/R)j_d$ and the experimentally determined U is much smaller than the theoretically predicted value.⁵ The differences between j_c and $(\xi/R)j_d$ may be ascribed to the uncertain values of λ and ξ in Eq. (1), effects of flux creep, and the unavoidable misalignment between the vortices and the columnar defects.³

The ideal parallel alignment of vortices and columnar defects usually discussed cannot be achieved in reality since the distance between two columnar defects is about 30 nm at a fluence $\phi t = 1 \times 10^{11}$ ions/cm²; this is smaller than the sample thickness by a factor of 10^3 for HTSC single crystals. Furthermore, the vortices are curved due to inhomogeneous demagnetization fields and pinning effects. Even when the angle φ between the defects and the vortices is small, the vortex lines will typically run through numerous columnar defects and not through a

single one as it is assumed in most existing theoretical models.⁷ In this situation sections of vortex lines are pinned by the columnar defects, but the connecting parts (kinks) are not pinned by the defect structure as shown in Fig. 1.

In order to find an adequate description of flux line depinning in samples with columnar defects two modes of vortex motion have to be considered:⁸ Usually, the vortex motion from one defect to another is assumed to occur by nucleation of kink pairs as shown for vortex 1 in Fig. 1. This motion can proceed in all directions. However, the vortex can also move by kink nucleation and kink sliding along the columnar defects if there is a finite angle between the vortices and these defects as shown for vortex 2. In most drift directions except the one perpendicular to the columnar defects this mode should even dominate over the vortex motion by kink pair nucleation. As a consequence, the introduction of columnar defects which are inclined to the sample surface should induce an in-plane anisotropy of the vortex motion and of the critical current density parallel and perpendicular to the direction of irradiation. Such an in-plane anisotropy can be observed directly only by local investigation techniques such as the magneto-optical Faraday effect which allows one to determine the local anisotropy ratio very exactly

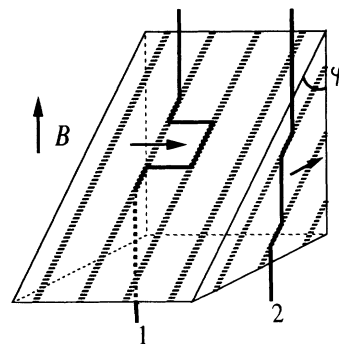


FIG. 1. Sketch of vortex motion crossing the columnar defects at an angle φ . Vortex 1 demonstrates the motion in perpendicular direction with nucleation of kink pairs. Vortex 2 moves due to kink sliding along the defects.

by measuring of distances in the critical state.⁹

In the present paper, results of direct observations of such an in-plane anisotropy by means of magneto-optical techniques will be presented, similar to the recent experiments on superconductors with crystallographic anisotropy.¹⁰ We were able to visualize two existing modes of vortex motion between columnar defects by direct local investigation of flux distributions in DyBa₂Cu₃O_{7- δ} (DBCO).

We use DBCO single crystals prepared as described in Ref. 11. The crystal dimensions are about $500 \times 500 \times 15 \mu\text{m}^3$ and $T_c \approx 88 \text{ K}$ as measured by the Meissner effect using superconducting quantum interference device (SQUID) magnetometry. All crystals have a distinct twin structure which was revealed by polarized light microscopy [see Fig. 2(a)].

Inclined columnar defects were introduced by irradiation with 0.9-GeV Pb ions at GANIL (Caen, France). The samples were glued on copper sample holders and mounted at various angles φ between the ion beam and the surface normal. The heavy ion irradiation lowers the critical temperature T_c by about 2 K at the fluences used.

To visualize the magnetic flux we use the magneto-optical Faraday effect in EuSe thin films. The full description of this magneto-optical technique is published in Ref. 12. The EuSe thin film was deposited on all single crystals before the irradiation. To reduce scatter of the sample properties all crystals were investigated magneto-optically before and after the irradiation. Dark areas on the photographs show the Meissner phase or regions where the magnetic field is lower than in the bright areas into which the normal component of the field has penetrated. We demonstrate the obtained results on a sample which was irradiated at an angle of $\varphi = 45^\circ$ with a fluence $\phi t = 1.41 \times 10^{11} \text{ ions/cm}^2$.

In Fig. 2(b) the flux distribution of the unirradiated sample in the critical state is shown at an external magnetic field of $\mu_0 H_{\text{ext}} = 256 \text{ mT}$ at $T = 30 \text{ K}$. The dark lines of the characteristic double Y form are clearly visible. This structure can be explained by the current distribution shown in Fig. 2(c). In the critical state a critical current of constant density j_c flows in the whole superconductor. A characteristic feature of such a vector field with a constant absolute value of the vector is the formation of sharp bends in the stream lines;¹³ this was discussed for type-II superconductors in the review by Campbell and Evetts.¹⁴ These bends occur at discontinuity lines of the current and divide the superconductor into domains with uniform parallel current flow. The characteristics of the discontinuity lines (d lines) under various geometric conditions and their experimental observation were described recently in Ref. 9. To fulfill the continuity condition for the critical current, the discontinuity lines form an angle of 45° with the edges of the rectangular sample in the isotropic case. This indeed is approximately the situation presented in Fig. 2(b) showing that the pinning force density was isotropic before irradiation.

Another feature revealed in Fig. 2(b) is the flux penetration along lines corresponding to the twin structure presented in Fig. 2(a). These brighter lines of higher

magnetic field are correlated with boundaries between regions of different twinning orientations. At these boundaries the end tips of the twin strips produce high internal stresses leading to a lower critical current density due to pressure effects, oxygen reduction, or local reduction of impurity concentration.

After these investigations the crystals were irradiated in the arrangement shown in Fig. 2(d). The irradiation

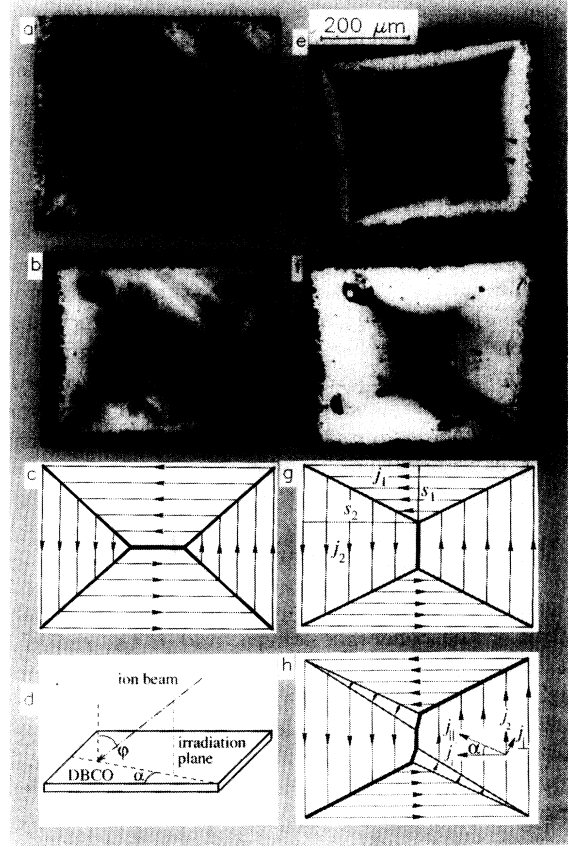


FIG. 2. Influence of angular lead irradiation on the flux structure of a DBCO single crystal. (a) Twin structure observed in polarized light. (b) Flux distribution in the critical state at $T = 30 \text{ K}$ and $\mu_0 H_{\text{ext}} = 256 \text{ mT}$ before the irradiation. (c) Sketch of the current distribution in the critical state of an isotropic, unirradiated, rectangular sample. (d) Schematic arrangement of the samples during the irradiation. The dash-dotted line indicates the direction of irradiation. (e) Flux penetration into the irradiated sample ($\varphi = 45^\circ$, $\alpha = 27^\circ$, $\phi t = 1.41 \times 10^{11} \text{ ions/cm}^2$) at $T = 30 \text{ K}$ and $\mu_0 H_{\text{ext}} = 512 \text{ mT}$. The white arrows indicate the direction of the incident ion beam, the black arrows show fingers of easier flux penetration. (f) The same at $T = 50 \text{ K}$ and $\mu_0 H_{\text{ext}} = 256 \text{ mT}$ in the critical state. (g) Known sketch of the current distribution in the critical state of an anisotropic sample ($j_1 > j_2$) (Ref. 15). (h) Analogical current distribution of general orientation of the anisotropy axes. The vector diagram shows the critical currents flowing parallel to the sample edges (j_1 , j_2) and the critical currents defined by the irradiation direction (j_{\parallel} , j_{\perp}). The magneto-optical images (b), (e), and (f) were revealed by an EuSe thin film at $T = 5 \text{ K}$ after cooling down from the indicated temperatures in applied magnetic field (Ref. 12).

tion increases the pinning in the samples. At $T = 30$ K we reached the critical state at $\mu_0 H_{\text{ext}} = 256$ mT in the unirradiated sample [Fig. 2(b)], whereas the regime of complete magnetization for the irradiated crystal has not been reached at our highest available magnetic field of $\mu_0 H_{\text{ext}} = 512$ mT at this temperature as shown in Fig. 2(e). Only at $T = 50$ K does the same field as in Fig. 2(b) $\mu_0 H_{\text{ext}} = 256$ mT produce the critical state [Fig. 2(f)]. Now, the central current discontinuity line in the characteristic double Y form is not oriented parallel to the longer side of the sample as in the isotropic case [Figs. 2(b) and 2(c)], but parallel to the shorter side. This picture is well known for anisotropic critical current densities¹⁵ as presented schematically in Fig. 2(g). It is clearly seen that the critical current density j_1 parallel to the long side of the sample is higher than the one parallel to the short side, j_2 . The ratio j_1/j_2 is obtained from the continuity condition $s_1 j_1 = s_2 j_2$, where s_1 and s_2 are the respective cross sections of the current flow divided by the constant sample thickness [see Fig. 2(g)]. From Fig. 2(f) we get $s_2/s_1 = j_1/j_2 \approx 2$.

Since the irradiation plane and the long side of the crystal include a small angle $\alpha = 27^\circ$, we cannot directly obtain the irradiation-induced anisotropy ratio j_{\parallel}/j_{\perp} between the critical currents flowing parallel (j_{\parallel}) and perpendicular (j_{\perp}) to the irradiation plane corresponding, respectively, to vortex motion perpendicular (vortex 1 in Fig. 1) and parallel (vortex 2 in Fig. 1) to the defects.

The easier flux penetration observed in the direction of irradiation, which is indicated by the black arrows in Figs. 2(e) and 2(f), shows that $j_{\perp} < j_2 < j_{\parallel}$. Note that the vortices move perpendicular to the critical current densities j_{\perp} and j_{\parallel} . Furthermore, the broader branches of the double Y structure in the upper left and lower right sample corner in Fig. 2(f) show that j_{\perp} is the lowest critical current density in the sample. The current density crossing the d lines is smaller than the critical current densities in adjacent domains due to the larger cross-sections. If this smaller value exceeds j_{\perp} , the double Y structure becomes unstable: The d lines where the current flows almost along j_{\perp} has to split into two d lines. Between the two d lines new domains with the homogeneous critical current density j_{\perp} appear [see Fig. 2(h)].

The appearance of the splitting can easily be understood from the following consideration: If we try to reduce the angle between the splitted d lines keeping the condition of current continuity, the current lines between these d lines shift towards the sample corner. This means an increase of the current density above the critical current density j_{\perp} , i.e., a destruction of the critical state. In Fig. 2(f) the broader d lines in the upper left and lower right part of the sample may be recognized as a small splitting of d lines. Figure 2(h) is drawn to reproduce schematically the situation presented in Fig. 2(f). From the small splitting of the d lines in Fig. 2(h) the ratio $j_1/j_{\perp} \approx 2.3$ is obtained by simple trigonometrical considerations taking into account that the tangential components of the stream lines at the d lines must be equal. The anisotropy ratio is thus concluded to be $j_{\parallel}/j_{\perp} \approx 2 - 3$, because j_1 is close to j_{\parallel} and j_2 is close to j_{\perp} .

It must be mentioned that the new pinning centers

introduced by irradiation mask the previous pinning features completely. In particular, the influence of twinning on the observed flux distribution has vanished. This fact can explain why sometimes the effect of twinning on the flux structures cannot be detected: In these cases most pinning centers within the sample are much stronger than the twin boundaries. This observation also indicates that the weak link behavior observed in the unirradiated sample is not due to reduction of superconductivity or to microcracks, but is caused by the formation of a channel of lower pinning in the boundary regions between different twin orientations. Further evidence of this claim follows from the observation that the introduction of new pinning centers removes the weak link behavior, which would not be possible if this were due to bad superconducting properties.

The formation of a completely new flux distribution after irradiation clearly shows that the columnar defects dominate the whole pinning behavior within the sample. The observed in-plane anisotropy demonstrates the existence of two modes of vortex motion and, furthermore, that sliding of kinks along the defects (see vortex 2 in Fig. 1) is definitely easier than kink pair nucleation (see vortex 1 in Fig. 1). From the depth of the flux penetration we can estimate the critical current densities in the sample.¹⁶ At $T = 50$ K j_1 was determined to $j_1 = 3 \times 10^6$ A/cm² and then j_{\parallel} was estimated to 5×10^6 A/cm². Since j_{\parallel} is the maximum current density in the sample—i.e., the vortices are oriented parallel to the columnar defects— j_{\parallel} should reach $(\xi/R)j_d \approx 6 \times 10^6$ A/cm² which is computed from Eq. (1).

What are the reasons for the deviations of j_{\parallel} from $(\xi/R)j_d$? Precise values of λ , ξ , and R which are required for a detailed comparison between theory and experiment are as yet unavailable. Furthermore, flux creep effects during the experiment reduce the measured critical current densities. Another possibility to explain the differences between j_{\parallel} and $(\xi/R)j_d$ could be the sliding of kink pairs along the columnar defects which is impeded by the fluctuating diameter and pinning potential (“sausaging”) along the columnar defects. Sliding of vortex kinks along linear or planar defects has been considered in numerous papers; see, e.g., Ref. 17.

Measurements of the temperature dependence of the anisotropy ratio, which will be published elsewhere, show that j_1/j_2 increases with increasing temperature. Thus, we can conclude that the pinning behavior is dominated by thermal activation. An interesting statistical theory of thermal depinning from randomly positioned linear defects has been given by Nelson and Vinokur.⁸

In conclusion, the observed in-plane anisotropy of flux pinning due to columnar defects shows the existence of *two* modes of vortex motion according to Fig. 1. It was found by magneto-optics that vortex 2 in Fig. 1 moves more easily than vortex 1. The determined critical current density j_{\parallel} is much lower than the calculated maximum critical current density $(\xi/R)j_d$. The reasons for this difference are discussed above. We believe that the critical current density in HTSC's with columnar defects is limited by thermal depinning and subsequent kink sliding along the defects.

The authors wish to thank Professor G. Saemann-Ischenko (Erlangen) and Dr. E. H. Brandt (MPI) for stimulating discussions. We are grateful to R. Henes and P. Keppler (MPI) for the sample preparation and to Dr. S. Bouffard (GANIL, Caen) and M. Kraus (Erlangen) for their assistance during the irradiation. We wish to thank E. Lutkat (MPI) for the preparation of the pho-

tographs. One of us (M.V.I.) is grateful to the Alexander-von-Humboldt-Stiftung for financial support. Part of this work was financially supported by the Bundesministerium für Forschung und Technologie and the Bayerischer Forschungsverbund Hochtemperatur-Supraleiter FORSUPRA. This is gratefully acknowledged.

-
- * Permanent address: Institute of Solid State Physics, Russian Academy of Sciences, Chernogolovka, 142432 Moscow distr., Russian Federation.
- ¹ B. Roas, B. Hensel, S. Henke, S. Klaumünzer, B. Kabius, W. Watanabe, G. Saemann-Ischenko, L. Schultz, and K. Urban, *Europhys. Lett.* **11**, 669 (1990).
 - ² L. Civale, A. D. Marwick, T. K. Worthington, M. A. Kirk, J. A. Thompson, L. Krusin-Elbaum, Y. Sun, J. R. Clem, and F. Holtzberg, *Phys. Rev. Lett.* **67**, 648 (1991).
 - ³ W. Gerhäuser, G. Ries, H. W. Neumüller, W. Schmidt, O. Eibl, G. Saemann-Ischenko, and S. Klaumünzer, *Phys. Rev. Lett.* **68**, 879 (1992).
 - ⁴ V. Hardy, J. Provost, D. Groult, M. Hervieu, B. Raveau, S. Durcok, E. Pollert, J. C. Frison, J. P. Chaminade, and M. Pouchard, *Physica (Amsterdam) C* **191**, 85 (1992).
 - ⁵ Th. Schuster, M. Leghissa, M. R. Koblishka, H. Kuhn, M. Kraus, H. Kronmüller, and G. Saemann-Ischenko, *Physica (Amsterdam) C* **202**, 203 (1992).
 - ⁶ M. Leghissa, L. A. Gurevich, M. Kraus, G. Saemann-Ischenko, and L. Ya. Vinnikov, *Phys. Rev. B* **48**, 1341 (1993).
 - ⁷ E. H. Brandt, *Europhys. Lett.* **18**, 635 (1992); *Phys. Rev. Lett.* **69**, 1105 (1992).
 - ⁸ D. Nelson and V. Vinokur, *Phys. Rev. Lett.* **68**, 2398 (1992); *Phys. Rev. B* **48**, 13060 (1993).
 - ⁹ Th. Schuster, M. V. Indenbom, M. R. Koblishka, H. Kuhn, and H. Kronmüller, *Phys. Rev. B* **49**, 3443 (1994).
 - ¹⁰ Th. Schuster, M. R. Koblishka, H. Kuhn, M. Glücker, B. Ludescher, and H. Kronmüller, *J. Appl. Phys.* **74**, 3307 (1993).
 - ¹¹ C. Thomsen, M. Cardona, B. Gegenheimer, R. Liu, and R. Simon, *Phys. Rev. B* **37**, 9860 (1988).
 - ¹² Th. Schuster, M. R. Koblishka, N. Moser, B. Ludescher, and H. Kronmüller, *Cryogenics* **31**, 811 (1991); M. V. Indenbom, Th. Schuster, M. R. Koblishka, A. Forkl, H. Kronmüller, L. A. Dorosinskii, V. K. Vlasko-Vlasov, A. A. Polyanskii, R. L. Prozorov, and V. I. Nikitenko, *Physica (Amsterdam) C* **209**, 259 (1992).
 - ¹³ H. A. M. van den Berg, *J. Appl. Phys.* **60**, 1104 (1986).
 - ¹⁴ A. M. Campbell and J. E. Evetts, *Critical Currents in Superconductors* (Taylor & Francis, London, 1972), p. 71; J. Evetts and A. M. Campbell, in *Concise Encyclopedia of Magnetic and Superconducting Materials*, edited by J. Evetts (Pergamon, Oxford, 1992), p. 100.
 - ¹⁵ E. M. Gyorgy, R. B. van Dover, K. A. Jackson, L. F. Schneemeyer, and J. V. Waszack, *Appl. Phys. Lett.* **55**, 283 (1989); F. M. Sauerzopf, A. P. Wiesinger, and H. W. Weber, *Cryogenics* **30**, 650 (1990).
 - ¹⁶ E. H. Brandt, M. V. Indenbom, and A. Forkl, *Europhys. Lett.* **22**, 735 (1993).
 - ¹⁷ C. A. Durán, P. L. Gammel, R. Wolfe, V. J. Fratello, D. J. Bishop, J. P. Rice, and D. M. Ginsberg, *Nature* **357**, 474 (1992); M. Turchinskaya, D. L. Kaiser, F. W. Gayle, A. J. Shapiro, A. Roytburd, V. Vlasko-Vlasov, A. Polyanskii, and V. Nikitenko, *Physica (Amsterdam) C* **216**, 205 (1993).

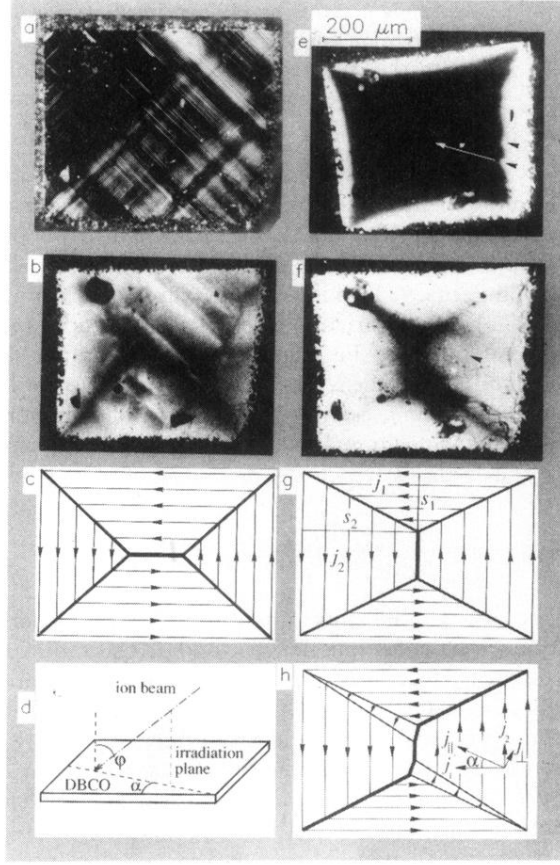


FIG. 2. Influence of angular lead irradiation on the flux structure of a DBCO single crystal. (a) Twin structure observed in polarized light. (b) Flux distribution in the critical state at $T = 30$ K and $\mu_0 H_{\text{ext}} = 256$ mT before the irradiation. (c) Sketch of the current distribution in the critical state of an isotropic, unirradiated, rectangular sample. (d) Schematic arrangement of the samples during the irradiation. The dash-dotted line indicates the direction of irradiation. (e) Flux penetration into the irradiated sample ($\varphi = 45^\circ$, $\alpha = 27^\circ$, $\phi t = 1.41 \times 10^{11}$ ions/cm²) at $T = 30$ K and $\mu_0 H_{\text{ext}} = 512$ mT. The white arrows indicate the direction of the incident ion beam, the black arrows show fingers of easier flux penetration. (f) The same at $T = 50$ K and $\mu_0 H_{\text{ext}} = 256$ mT in the critical state. (g) Known sketch of the current distribution in the critical state of an anisotropic sample ($j_1 > j_2$) (Ref. 15). (h) Analogical current distribution of general orientation of the anisotropy axes. The vector diagram shows the critical currents flowing parallel to the sample edges (j_1, j_2) and the critical currents defined by the irradiation direction (j_{\parallel}, j_{\perp}). The magneto-optical images (b), (e), and (f) were revealed by an EuSe thin film at $T = 5$ K after cooling down from the indicated temperatures in applied magnetic field (Ref. 12).